A Digital Anemometer

Ken Okamoto, Tadahiko Ohhashi, Masahiro Asakura, and Kenzo Watanabe, *Fellow, IEEE*

***Abstract*—A digital anemometer has been developed for air flow measurements in home and office environments. The principle is based on hot-wire anemometry. The probe consists of a cold thermistor for flow temperature detection and a hot thermistor for flow rate detection. The latter is self-heated by a thermal bridge. Its unbalance voltage due to the air flow is compared with the reference response transformed into the time domain by direct digital synthesizing. This pulse-width modulation provides the linear digital representation of the flow rate under measurement. The unbalance component due to flow temperature is compensated by scaling the reference response depending on temperature detected by a cold thermistor. These linearization and compensation techniques make accurate measurements possible with a simple configuration. Performances of a prototype anemometer built using a one-chip 4-bit microcomputer are also presented to demonstrate the validity of these techniques.**

I. Introduction

BESIDES temperature and humidity control, air flow control is increasingly demanded to make home, office, and working environments more comfortable. Many methods are available for unidirectional laminar flow measurements [1], but a hot-wire anemometry is exclusively used for measurements of the turbulent flow in open space [2]. A hot-wire anemometer is basically a thermal transducer which measures the fluid speed by detecting its resistance change when exposed to a cross flow. Therefore, any thermoresistive device can be used for the transducer [3], [4], but the most common is a fine platinum wire called the Wollaston wire. Its resistance changes, due to the heat removed by the fluid flow, have been investigated extensively and are expressed by the King's law [5].

Another typical device used for thermoanemometry is a thermistor. This thermoresistive temperature sensor is much cheaper than the Wollaston wire and thus is attractive for a low-cost, air flow controller for fans and air conditioners. The design and realization of a thermistor-based anemometer present, however, three main difficulties. The first is the slow response due to its long thermal time constant. The second is the highly nonlinear resistance change with temperature, and the third, which is common to a Wollaston-wire system, is the complex dependence of the heat transfer on fluid temperature [6].

These three problems have been examined from device and signal-processing aspects. The first problem has been solved by developing a miniature thermistor whose thermal time constant is ten times shorter with respect to a conventional device. A response speed comparable to a Wollaston-wire system can be obtained by working in the constant-temperature mode. For linearization, the pulse-width-modulation (PWM) technique is used. Different from a conventional sawtooth, the carrier signal to be modulated is the thermistor response to flow rate transformed into the time domain by the direct digital synthesizing (DDS) technique [7]. The third problem, i.e., temperature compensation, is solved by scaling the carrier waveform appropriately depending on fluid temperature. A high-performance digital anemometer realized by these techniques will next be described in detail.

Manuscript received May 18, 1993; revised October 8, 1993.

K. Okamoto, T. Ohhashi, and M. Asakura are with the Development Laboratory, Kurabe Industrial Corporation, Hamamatsu, 432 Japan.

K. Watanabe is with the Research Institute of Electronics, Shizuoka University, Hamamatsu, 432 Japan.

IEEE Log Number 9215989.

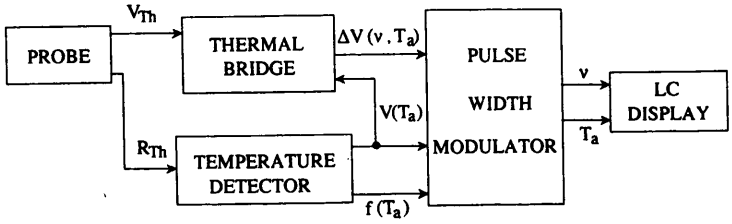

Fig. 1. The block diagram of the digital anemometer.

II. Configuration of Anemometer

A block diagram of the digital anemometer is shown in Fig. 1. It consists of the probe exposed to a cross flow, the thermal bridge to convert the air flow velocity into a voltage signal, the temperature detector to convert the flow temperature into its proportional voltage, the pulse-width modulator (PWM) to convert the thermal bridge output into a digital number equivalent to the flow rate, and the liquid crystal display (LCD) to indicate air flow rate and temperature in 3-digit form. Each block is next described in more detail with emphasis on the process of linearization and temperature compensation.

A. Probe

The configuration of the probe is shown in Fig. 2. It is composed to two matched miniature thermistors, 0.9 mm in diameter and 1.2 mm long, welded to stainless-steel stays. Its resistance $R_{\mathrm{Th}}(T)$ at temperature T follows a conventional exponential law expressed by

$$R_{\mathrm{Th}}(T) = R(T_r) \exp B\left(\frac{1}{T} - \frac{1}{T_r}\right). \quad (1)$$

The B constant and the resistance $R(T_r)$ at the reference temperature $T_r = 298\mathrm{K}$ are 3390K and 5.46 kΩ, respectively. Because of the small size, the thermal time constant at high temperature is about 0.2 s, which is ten times shorter with

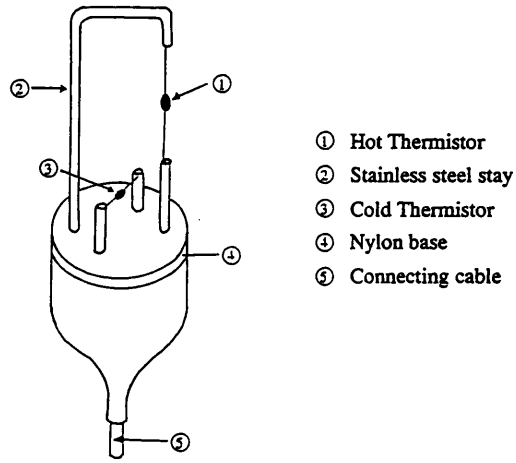

Fig. 2. The configuration of the probe.

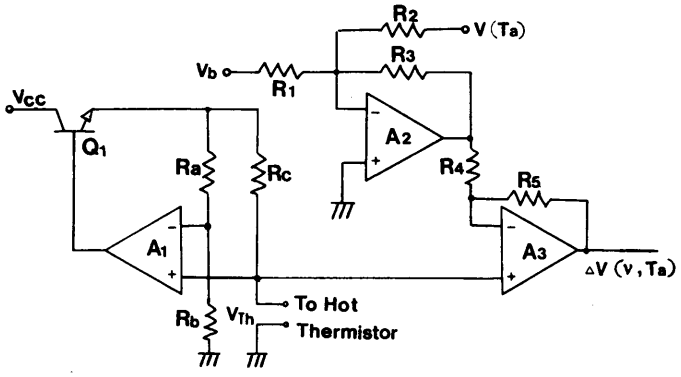

Fig. 3. The circuit diagram of the thermal bridge.

respect to a conventional thermistor [8]. One of the thermistors is self-heated to 423K for flow rate measurements. It is hung by long lead wires away from the stays in order to avoid any influence to the flow field to be measured. The large thermal resistance of the leads also reduces the heat lost by end conduction to a minimum. The other thermistor is used for detecting the flow temperature. It is located away from the hot thermistor so it also leaves the flow field unchanged.

B. Thermal Bridge

Fig. 3 shows the circuit diagram of the thermal bridge. The thermistor for flow rate detection is connected to one arm of the Wheatstone bridge which is placed in the feedback circuit formed by the op-amp A_1 and the transistor Q_1. The feedback circuit biases the bridge in such a way that its balance can be maintained. The resistance of the thermistor is thus kept constant, and hence it operates in the constant-temperature mode. The resistors of the Wheatstone bridge are selected such that the thermistor temperature be 423K.

To derive the characteristic function, the voltage $V(\nu, T_a)$ across the hot thermistor was measured as a function of air flow rate ν and temperature T_a. The results are plotted in Fig. 4. It was found from these results that $V(\nu, T_a)$ can be expressed as follows:

$$\begin{aligned} V(\nu, T_a) &= V(\nu, T_r)g(T_a) \\ &= \{V(0, T_r) + \Delta V(\nu, T_r)\}g(T_a) \\ &= \{V(0, T_r) + h(\nu, T_r)V_r\}g(T_a) \end{aligned} \quad (2)$$

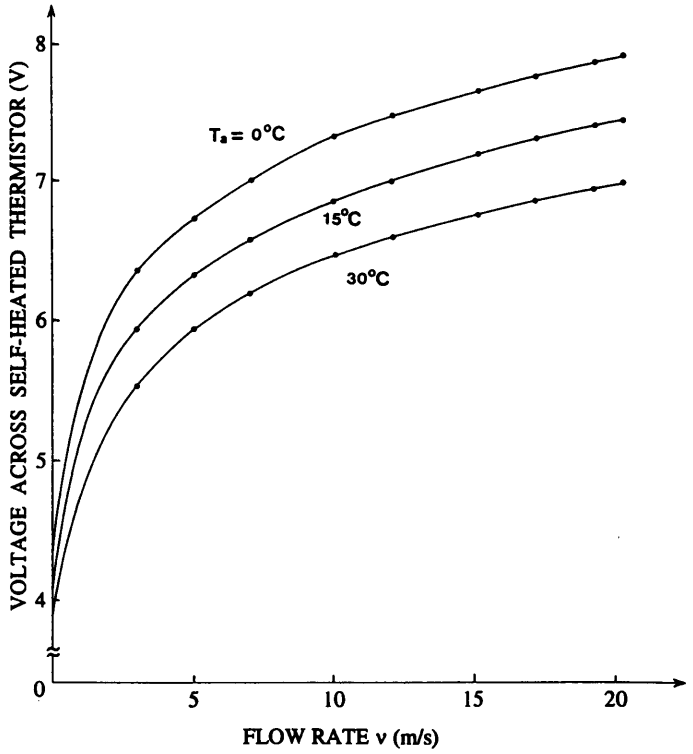

Fig. 4. The voltage across the thermistor operating in the constant-temperature mode.

where $V(0, T_r)$ and $\Delta V(\nu, T_r)$ denote the offset and unbalance components, respectively, at some reference temperature T_r. The temperature dependence $g(T_a)$ at $T_r = 300$K is given by

$$g(T_a) = 1 + 4.28 \times 10^{-3}(T_r - T_a). \quad (3)$$

Because of the exponential behavior of the thermistor resistance, the characteristic function $h(\nu, T_r)$, which can be obtained by normalizing the unbalance voltage $\Delta V(\nu, T_r)$ with a reference voltage V_r, deviates from the King's law and is approximated by a logarithmic function of flow rate ν :

$$h(\nu, T_r) = \frac{\alpha}{\ln \nu - \beta} \quad (4)$$

where α and β are constants. The characteristic function at $T_r = 300$K, normalized with reference to $V_r = 2$ V, is shown in Fig. 5.

The offset components $V(0, T_r)g(T_a)$ is redundant because it carries no information of the flow rate. The op-amp A_2 is used to cancel it. Driven by a fixed voltage V_b and the temperature-dependent voltage $V(T_r)$, available from the temperature detector, it produces the output voltage which counterbalances $V(0, T_r)g(T_a)$ over a wide temperature range. Op-amp A_3 thus provides only the unbalance signal $\Delta V(\nu, T_r)g(T_a)$ to the PWM.

C. Temperature Detector

The temperature detector consists of a linear temperature-to-frequency (T/F) converter followed by a frequency-to-voltage (F/V) converter [9]. The circuit diagram of the T/F converter

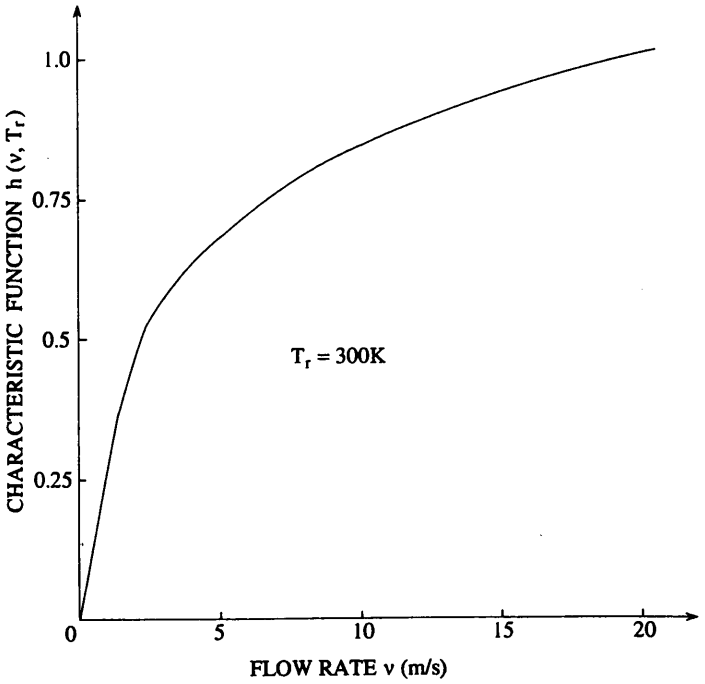

Fig. 5. The characteristic function $h(\nu, T_r)$ at $T_r = 300K$.

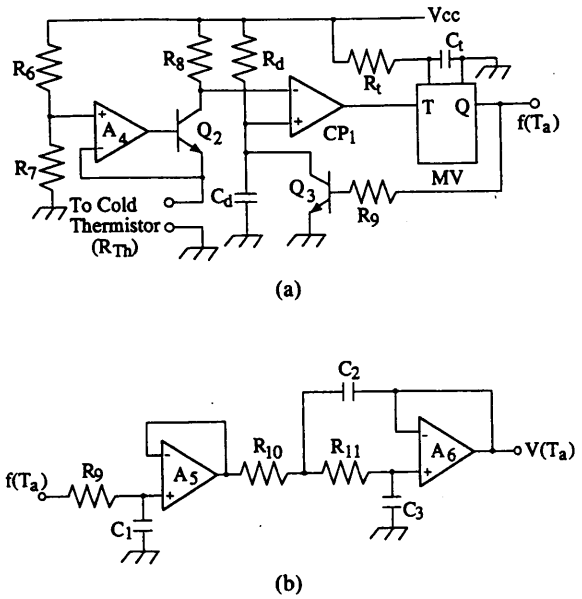

Fig. 6. Circuit diagrams of (a) the temperature-to-frequency converter and (b) the frequency-to-voltage converter in the temperature detector.

is depicted in Fig. 6(a). The cold thermistor in the probe is connected between the emitter of Q_2 and ground. Due to the feedback to op-amp A_4, the voltage across the cold thermistor is kept constant, and thus the current flowing through Q_2 increases exponentially with temperature, producing the temperature-dependent collector voltage given by

$$V_T = V_{cc}(1 - kR_8/R_{\mathrm{Th}}(T)), \tag{5}$$

where $k = R_7/(R_6 + R_7)$, and $R_{\mathrm{Th}}(T)$ is the resistance of the cold thermistor given by (1).

The capacitor C_d is charged exponentially through R_d until its voltage reaches V_T. At this instant, the monostable multivibrator (MV) is triggered and discharges C_d via Q_3. After a period τ_m when the output of MV goes low, the charge process of C_d toward V_{cc} is started again. The time τ_c required for charging C_d to V_T is given by

$$\tau_c = C_d R_d \left[\ln \frac{R(T_r)}{kR_8} + \frac{B}{T} - \frac{B}{T_r}\right]. \tag{6}$$

By setting the pulse width τ_m of MV such that

$$\tau_m = C_d R_d \left(\frac{B}{T_r} - \ln \frac{R(T_r)}{kR_8}\right) \tag{7}$$

holds, one can get the linear relation between the output frequency $f(T_a)$ and temperature T_a :

$$f(T_a) = \frac{1}{\tau_c + \tau_m} = \frac{T_a}{C_d R_d B}. \tag{8}$$

The output of the T/F converter is the pulse train with constant width τ_m. Therefore, the output frequency $f(T_a)$ is easily converted into its proportional dc voltage $V(T_a)$ by means of low-pass filtering. The circuit diagram is shown in Fig. 6(b). R_9 and C_1 form the low-pass filter (LPF) for the F/V conversion. The single-amplifier biquad formed by op-amp A_6 follows the LPF to reject the ripple component. Assuming that the time constant R_9C_1 is greater than the period of the lowest possible frequency of $f(T_a)$, the output voltage $V(T_a)$ of op-amp A_6 is given by

$$V(T_a) = f(T_a)\tau_m V_\tau = \frac{\tau_m V_\tau}{C_d R_d B} T_a, \tag{9}$$

where V_τ is the amplitude of the frequency signal $f(T_a)$.

D. Pulse-Width Modulator

Fig. 7 shows the functional diagram of the PWM. The ROM stores the characteristic function $h(\nu, T_r)$ in table form, with ν being the table address i. This table is read out sequentially by accessing the ROM using the incremental address counter. Data are converted into the carrier signal of the PWM by the digital-to-analog (D/A) converter. This process of direct digital synthesizing (DDS) transforms the characteristic function in the ν domain into the time domain. The carrier signal $h(i, T_r)V_{\mathrm{ref}}$ thus produced is compared with $\Delta V(\nu, T_a)$ by the comparator CP_2. When both the signals coincide, CP_2 issues the reset signal ϕ_R to store the table address i into the register. The address i then gives the digital equivalent of the flow rate ν. To reduce the table size, only the characteristic function at the reference temperature T_r is stored. Compensation for the air flow temperature T_a is made by introducing the temperature dependence $g(T_a)$ into the reference voltage V_{ref} via $V(T_a)$.

The table size can be determined as follows. The address is the digital equivalent of the flow rate. Thus, the address size is determined by the resolution required over the full-scale

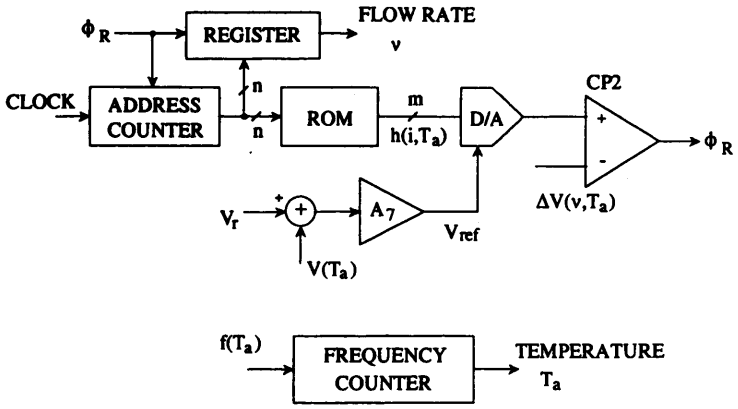

Fig. 7. The functional diagram of the pulse-width modulator.

range. The data length can be derived from the sensitivity of $h(\nu, T_r)$ to ν :

$$S_\nu^h = \frac{\partial \ln h(\nu, T_r)}{\partial \nu} = \frac{1}{\ln \nu - b}. \tag{10}$$

The sensitivity decreases with ν, as can also be seen from the slope of the characteristic function shown in Fig. 5, to be 1/4 at $\nu_{\max} = 20$ m/s. This implies that the quantization of $h(\nu, T_r)$ should be four times finer than that of ν. Therefore, the data length should be 2 bits wider than the address size.

The PWM also includes the frequency counter which counts $f(T_a)$ to display the air temperature T_a with 0.1K resolution. The flow rate ν and temperature T_a thus measured are displayed on the 3-digit LCD.

III. Prototype Anemometer

A prototype anemometer was breadboarded using off-the-shelf components except for the probe. To reduce the component count and thereby to ease the assembly, all the digital functions necessary for the DDS were implemented by a one-chip 4-bit microcomputer. It includes, besides many other facilities, 512 × 4-b RAM and 4K × 8-b ROM. The 3-digit LCD drive facility and a frequency counter are also accommodated.

The specified resolution is 0.1 m/s over the full-scale range of 20 m/s. Therefore, 10 bits are enough for the data length of the table, but the characteristic function was quantized into 12-bit words for better accuracy and wider range. Since one word occupies 2 bytes, 400 bytes of the ROM were allotted to the characteristic table. Each word is sent to a multiplying 12-bit D/A converter via three 4-bit ports. The time required by the software to scan the table, send it to the D/A converter, acquire the reset signal ϕ_R, and then convert the table address into the LCD code is 140 ms. To evaluate its performances, the prototype anemometer was applied to air flow rate measurements in a wind tunnel. The flow rate indicated on the LCD was compared with that measured by a commercial manometer. Errors between them are plotted in Fig. 8. In the constant-temperature anemometer, the error due to convection is inevitable. Despite this error source, the errors are within ±2 %FS over the temperature range from 0°C to 30°C. These results prove the present anemometer useful for most applications.

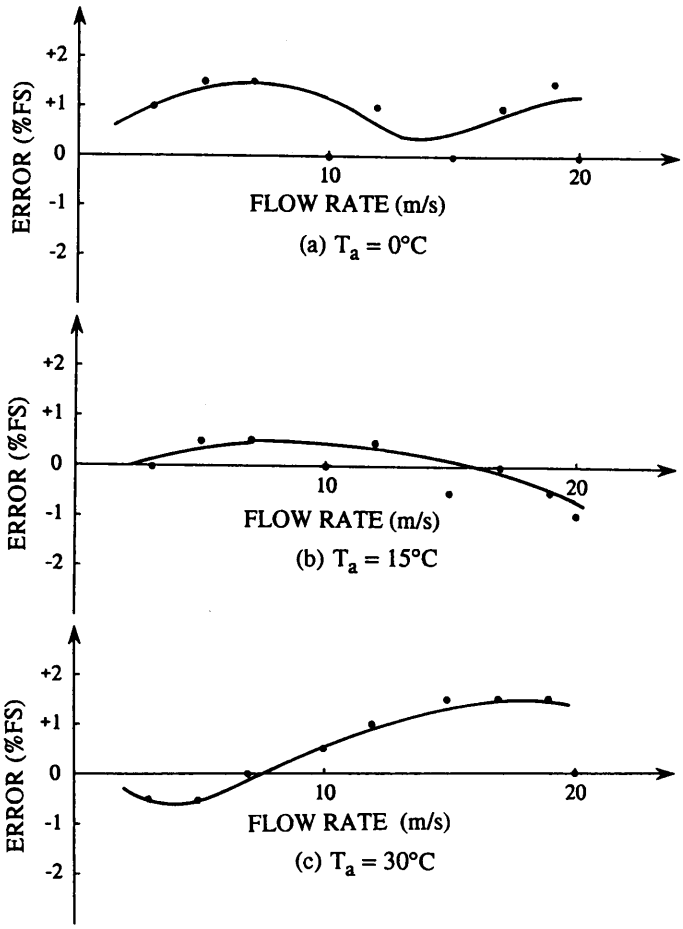

Fig. 8. Errors between readings of the prototype anemometer and manometer.

IV. Conclusions

A constant-temperature anemometer using miniature thermistors was described. It provides the linear digital output by comparing the voltage across the self-heated thermistor with the characteristic waveform generated by the direct digital synthesizing technique. Temperature compensation was also accomplished by introducing the same temperature dependence into the DDS waveform as that of the thermistor voltage. The prototype anemometer using a one-chip 4-bit microcomputer for compact implementation has confirmed the validity of these techniques.

Because of its high performance/cost ratio, the anemometer described herein will find wide applicability in air conditioning. Incorporating the humidity measurement capability is a future work toward environment monitors and controllers.

References

[1] A. Boros, *Electrical Measurements in Engineering*. Amsterdam: Elsevier, 1985, ch. 6 and 9.
[2] A. E. Perry, *Hot-Wire Anemometry*. Oxford, UK: Clarendon, 1982.
[3] A. Catellani, R. Stacchietti, A. Taroni, and C. Canali, "Performance and temperature stability of an air mass flowmeter based on a self-heated thermistor," *Sensors and Actuators*, vol. 3, pp. 23–30, 1982/1983.
[4] Y. Pan and J. H. Huijsing, "New integrated gas-flow sensor with duty cycle output," *Electron. Lett.*, vol. 24, pp. 542–543, Apr. 1988.

[5] L. V. King, "One the convection of heat from small cylinders in a stream of fluid: Determination of the convection constants of small platinum wires with application to hot-wire anemometry," *Proc. Royal Soc. London,* vol. 90, pp. 563–570, 1914.
[6] C. Yang, M. Kümmel, and H. Soeberg, "A self-heated thermistor flowmeter for small liquid flow in microchannels," *Sensors and Actuators,* vol. 15, pp. 51–62, 1988.
[7] M. Yamada, T. Takebayashi, S. Notoyama, and K. Watanabe, "A sensor signal processor," in *IEEE Instr. Meas. Technol. Conf. Rec.,* 1992, pp. 400–403.
[8] "Small NTC thermistors; S series," Kurabe Technical Note, Cat No. N-148, Kurabe Industrial Corp., 4830 Takatsuka, Hamamatsu, Japan.
[9] O. I. Mohamed, T. Takaoka, and K. Watanabe, "A simple linear temperature-to-frequency converter using a thermistor," *Trans. IEICE,* vol. E70, pp. 775–778, Aug. 1987.

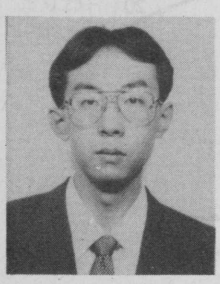

Ken Okamoto received the B.Eng. degree from Shizuoka University, Hamamatsu, in 1990.

Upon graduation, he joined Kurabe Industrial Corporation, Ltd., Hamamatsu and is now engaged in the development of measurements and control circuits in the Development Laboratory.

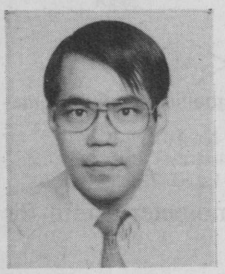

Tadahiko Ohhashi received the B.Eng. degree from Niigata University, Niigata, Japan, in 1980.

He joined Kurabe Industrial Co., Ltd., Hamamatsu, Japan, in 1980, and is now engaged in research and development of measuring equipments.

Masahiro Asakura received the B.Eng. degree from Gunma University, Gunma, Japan, in 1967.

Upon graduation, he joined NEC where he was engaged in the development of semiconductor power devices. In 1975, he moved to Shibaura Electric Corporation Ltd., where he was engaged in the development of temperature and humidity detectors. In 1984, he joined Kurabe Industrial Corporation, Ltd., where he is managing the Development Laboratory.

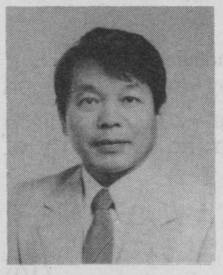

Kenzo Watanabe (M'74–SM'86–F'93) received the B.E. and M.E. degrees in engineering from Shizuoka University in 1962 and 1966, respectively, and the Dr.Eng. degree from Kyoto University in 1976.

He is a Professor of the Research Institute of Electronics, Shizuoka University, Hamamatsu, Japan. Except for a year as a Visiting Professor at UCLA, he has been on the faculty at Shizuoka University since 1962, serving progressively as Research Assistant, Associate Professor and Professor.

Dr. Watanabe serves IEEE activities as an AdCom member of IM Society, an Associate Editor of *Transactions on Instrumentation and Measurement*, and a Vice Chairman of IM Tokyo Chapter.